JOURNAL OF MATERIALS SCIENCE **40** (2005) 5609–5618

Fracture and failure behavior of basalt fiber mat-reinforced vinylester/epoxy hybrid resins as a function of resin composition and fiber surface treatment

T. CZIGÁNY*, K. PÖLÖSKEI
Department of Polymer Engineering, Faculty of Mechanical Engineering,Budapest University of Technology and Economics, Budapest, H-1111, Mügyetem rkp. 3., Hungary
E-mail: czigany@eik.bme.hu

J. KARGER-KOCSIS
Institut für Verbundwerkstoffe GmbH, Technische Universität Kaiserslautern, D-67663, Kaiserslautern, Germany

Published online: 25 August 2005

The mechanical and failure behaviour of basalt fiber (BF) mat-reinforced (30 wt%) composites with vinylester (VE) and vinylester/epoxy (VE/EP) hybrid resins were studied as a function of resin hybridization (VE/EP = 3/1, 1/1 and 1/3) and BF surface treatment. BF was treated either with vinyl or epoxy functionalized organosilanes (VS and ES, respectively). The VE/EP hybrids exhibited an interpenetrating network (IPN) structure in the studied composition range. Specimens, cut of plaques produced by resin transfer molding (RTM), were subjected to static (tensile, flexural) and dynamic (instrumented Charpy and falling weight impact) loading. The fracture toughness was determined under both static and dynamic conditions. The development of the damage zone and its propagation were followed by location of the acoustic emission (AE). It was found that the mechanical properties of the composites were strongly improved when mats with treated BF surface were incorporated. This was mostly traced to the good interfacial adhesion between the BF and matrix according to fractographic inspection. The formation of the interphase (ca. 2 μm thick) was influenced by the BF treatment: VS coating of the BF resulted in VE-, whereas ES-treatment in EP-enrichment in the interphase due to which the IPN structure also changed locally. This was demonstrated by nanoindentation measurements performed with an atomic force microscopy (AFM) on ion-ablated polished surface specimens.
© *2005 Springer Science + Business Media, Inc.*

1. Introduction

Polymer composites are nowadays typically reinforced by glass fibers (GF). GF has high modulus, good strength, exhibits acceptable adhesion towards various polymer matrices, and, at the same time it is low priced [1]. In more demanding applications carbon fiber (CF), outperforming GF in respect with stiffness and strength, is used. However, CF is markedly more expensive than GF, and the proper adhesion between CF and polymer matrix is also not easy to realize in many cases [2]. Recently a new type of reinforcing fiber with excellent mechanical properties, produced from basic volcanic rock by melt technology, the so-called basalt fiber (BF), appeared [3]. Discontinuous BFs produced by the Junkers melt-blowing technology are very brittle and thus not yet widely adopted for the production of polymer matrix-based composites. It was reported that new technologies have to be developed to avoid the breakage of BF during all steps of processing as fiber attrition is associated with severe property degradation [4]. Much better composite properties can be achieved if a BF perform, such as mat, is impregnated with a thermoset resin. The fracture of BF can be circumvented by applying resin infiltration techniques, such as resin transfer molding (RTM) [5].

Therefore the aim of this study was to produce BF mat-reinforced thermoset polymer composites containing vinylester (VE) and vinylester/epoxy (VE/EP) hybrid resins as matrices, and to investigate their fracture and failure properties. VE has been

*Author to whom all correspondence should be addressed.
0022-2461 © *2005 Springer Science + Business Media, Inc.*
DOI: 10.1007/s10853-005-1273-8

chosen owing to its superior mechanical and chemical resistance as compared to unsaturated polyesters. The application of VE/EP resin combinations is justified by the necessity of the surface treatment of BF which is the major learning from the literature [6]. Note that basalt fibers act as reinforcing ones in polymer composites only after their surface treatment. EP resins are widely used as matrix materials in thermoset composites [7], so it is not by chance that EP-sized fibers (e.g., GF and CF) are well-introduced products on the market. The same cannot be said about VE resins, which fiber-matrix adhesion problems are often detected with. Therefore the incorporation of an EP-sized fiber into a VE/EP resin may be very advantageous and effective to achieve good interfacial adhesion. This is favored by the special morphology of the VE/EP resins. It has been demonstrated by atomic force microscopic (AFM) studies that these hybrid resins are of interpenetrating network (IPN) structure [8–10].

In order to ensure the proper adhesion between the fiber and matrix in the composites, the reinforcing fibers should be surface treated. This improves the strength of the composite, however, usually at cost of the toughness. Therefore several research groups have dealt with the problem how to improve the interfacial adhesion in order to get balanced stiffness, strength/toughness properties. The strategies followed so far in this direction tackled the reinforcing fibers, more exactly their coating. It has been suggested [11, 12] to change the surface treatment periodically along the length of the fiber. An alternative way, viz. to approach the problem from the matrix-side, was proposed only recently. Note that via an IPN structure an intermittent bonding between fiber and matrix can be achieved per se, if the initial IPN structure is not affected by the presence of the fiber reinforcement. The IPN structure ensures the periodical change in the fiber/matrix adhesion along the interface on nanometer scale. This matrix-induced intermittent bonding may allow us to produce composites showing high strength and high toughness at the same time [13, 14].

2. Experimental

The vinylester (VE) resin grade used in our study was Daron XP-45 A2 (DSM Composite Resin, The Netherlands), which is a reaction product of bisphenol A and methacrylic acid and it contains 30 wt% styrene. Styrene is an active diluent in this case. Active, as it is a co-monomer of the radical crosslinking of the vinylester resin and it is a diluent, as it reduces the viscosity of the vinylester resin considerably. As a consequence of the latter, the resin becomes especially suitable for RTM processing. The radical initiator of the VE/styrene crosslinking process was dibenzoyl-peroxide (0.75 phr), the accelerator was N,N-diethyl aniline (0.15 phr). The epoxy resin grade used was aliphatic Polypox R3 (1,4-butanediol-diglycidylether, manufacturer: U. Prümer Polymer Chemie GmbH, Germany). The crosslinker was a cycloaliphatic diamine, HY 2954 (2,2′-dimethyl-4,4′-methylene-bis(cyclohexylamine), manufacturer: Hunstman GmbH, Germany).

A BF-mat of Toplan Ltd. (Hungary) served as reinforcement (average fiber diameter: 9 ± 2 μm, fiber length: 10–50 mm). The fiber content was ca. 30 wt% in each composite. BF was surface treated with two types of organosilanes. One of the coupling agents contained epoxy functional groups (3-(glycidyloxypropyl)trimethoxysilane, ES), while the other vinyl functionality (3-(trimethoxysilyl)propyl-methacrylate, VS) in order to improve the adhesion of BF towards either EP or VE. Both VS and ES were products of Aldrich Co., Germany. Treatment of the BF mats was made by dissolving the silanes in distilled water (1 wt% solution), then the mats were immersed in the aqueous solution for 2 h, followed by drying at 50°C for four days. The VE/EP ratios set were 1/3, 1/1 and 3/1. This selection was due to the fact that the IPN structure is still present in the above range [15], and the composite properties can be varied by this way within a broad range.

The aluminium mold (home-made) was designed to be filled by the resin easily and to fit into a thermostat where the crosslinking was performed. Filling of the evacuated mold occurred by 1 bar pressure to avoid the formation of air bubbles in the molded plaques. The temperature program of the crosslinking process was 80°C for 3 h followed by 150°C for 3 h. The composition of the composites is summarized in Table I. Accordingly, the properties of composites were studied as a function of the resin hybridization (affecting also the IPN structure), and BF surface treatment.

Standard static and dynamic mechanical tests were used to determine the mechanical properties of the composites. Specimens were cut from the 3 mm thick plaques by an Emcostar diamond-disk sawing machine. The size tolerance during machining of the specimens was ±0.2 mm. The actual size of the samples was measured accordingly on each specimen before testing. Tests were performed on 5 parallel specimens at room temperature, and the averages and standard deviations were calculated for the corresponding property.

TABLE I Composition of the composite samples prepared with thermoset matrices

	Resin composition	BF content (m%)	Treatment
K1	VE	0	–
K2	VE	30	–
K3	VE	30	VS
K4	VE	30	ES
K5	VE/EP 1/1	0	–
K6	VE/EP 1/1	30	–
K7	VE/EP 1/1	30	VS
K8	VE/EP 1/1	30	ES
K9	VE/EP 3/1	0	–
K10	VE/EP 3/1	30	–
K11	VE/EP 3/1	30	VS
K12	VE/EP 3/1	30	ES
K13	VE/EP 1/3	0	–
K14	VE/EP 1/3	30	–
K15	VE/EP 1/3	30	VS
K16	VE/EP 1/3	30	ES

Notes, designations: K1, K5, K9 and K13 do not contain reinforcement, VE-vinylester, EP-epoxy resin, VS-vinylsilane, ES-epoxysilane.

2.1. Static mechanical tests

Tensile tests were performed according to the EN ISO 527 standard, on a Zwick Z050 tensile tester. From the force-elongation curves measured on rectangular samples of 150 mm length and 20 mm width, the tensile strength (σ_{tensile}) and the tensile modulus (E_{tensile}) were calculated. To avoid the slippage of the specimens from the clamps and the breakage of the specimens at the clamping the specimens were tabbed by 2 mm thick and 35 mm length inserts. Tabs were prepared from glass fabric reinforced polyester resin and fixed onto the samples by Sika Dur 4400 adhesive.

Three-point bending tests were performed in accordance with the EN ISO 14125 standard on a Zwick Z020 tester. The length, span length and width of the specimens were 70, 48 and 20 mm, respectively. From the load-deflection curves the bending strength (σ_{bending}) and the bending modulus (E_{bending}) were calculated.

Fracture mechanical tests were conducted on 110 mm long and 30 mm wide, single-edge notched tensile loaded (SEN-T) specimens (notch length ca. 10 mm). The notch root was sharpened by a razor blade before testing. The critical stress intensity factor or fracture toughness (K_{ICstat}) was determined from the load-deformation curves registered by a Zwick Z020 tester [16] (1).

$$K_{\text{ICstat}} = \frac{F_{\max}}{B \cdot W} \cdot \mathrm{a}^{1/2} \cdot f(\mathrm{a/W}) \tag{1}$$

where $F_{\max}$ is the maximum force, B is the thickness of the specimen, W is its width, a is the crack length including the sawed notch length and the razor-cut crack, f is the geometrical correction factor, which can be determined by Equation 2:

$$f(a/W) = 1.99 - 0.41(a/W) + 18.7(a/W)^2 - 38.48(a/W)^3 + 53.85(a/W)^4 \tag{2}$$

The tensile, three-point bending and fracture toughness tests were performed at 1 mm/min deformation rate at room temperature.

2.2. Dynamic mechanical tests

Charpy tests were performed on an instrumented CEAST Resil Impactor Junior pendulum impact tester. A 15 J hammer was used at 3.3 m/s velocity. According to the prescriptions of the ISO 179 standard 100 mm long and 20 mm wide specimens with 5 mm notch length were used (span width: 80 mm). The notch of the specimens was sharpened by pressing a razor blade. From the test results the dynamic stress intensity factor (K_{ICdyn}) was calculated using Equations 3 and 4 [17], where a is the total crack length and $\alpha = a/W$.

$$K_{\text{ICdyn}} = \frac{F_{\max}}{B \cdot W} \cdot a^{1/2} \cdot f(a/W) \tag{3}$$

$$f(a/W) = 6\alpha^{1/2} \frac{[1.99 - \alpha(1-\alpha) \cdot (2.15 - 3.93\alpha + 2.7\alpha^2)]}{(1+2\alpha) \cdot (1-\alpha)^{3/2}} \tag{4}$$

The specific crack-propagation energy (G_{IC}) was calculated according to (5), where Φ, A and $dA/d\alpha$ are correction factors, see Equation (6)–(8):

$$G_{\text{IC}} = \frac{E_{F_{\max}}}{BW\phi} \tag{5}$$

$$\phi = \frac{A + 18.64}{dA/d\alpha} \tag{6}$$

$$A = \frac{16\alpha^2}{(1-\alpha)^2}[8.9 - 33.717\alpha + 79.616\alpha^2 - 112.952\alpha^3 + 84.815\alpha^4 - 25.672\alpha^5] \tag{7}$$

$$dA/d\alpha = \frac{16\alpha^2}{(1-\alpha)^2}[-33.717 + 159.232\alpha - 338.856\alpha^2 + 339.26\alpha^3 - 128.36\alpha^4] + 16 \cdot [8.9 - 33.717\alpha + 79.616\alpha^2 - 112.952\alpha^3 + 84.815\alpha^4 - 25.672\alpha^5] \cdot \left[\frac{2\alpha(1-\alpha) + 2\alpha^2}{(1-\alpha)^3}\right] \tag{8}$$

The specific facture energy (impact strength – a_{cN}) was calculated by:

$$a_{cN} = \frac{E_{\max}}{B \cdot (W - a)} \tag{9}$$

where $E_{\max}$ is the total fracture energy.

Instrumented falling weight impact (dart drop) tests were performed using a CEAST Fractovis 6785 instrument. Quadratic specimens (60 × 60 mm^2) cut of the plaques were hit by the dart (diameter: 20 mm, mass: 7.5 kg, incident velocity: 10 m/s velocity). From the test results the energy-absorbing ability (ductility ratio, D_r) and the specific perforation energy needed to break through the composite sheets (E_p) were calculated by Equations 10 and 11 [18]:

$$\mathrm{D_r} = \frac{\mathrm{E_{max}} - E_{F_{\max}}}{\mathrm{E_{max}}} \cdot 100\,[\%] \tag{10}$$

$$\mathrm{E_p} = \frac{E_{\max}}{B} \tag{11}$$

where $E_{F\max}$ is the energy at the maximum force, B is the thickness of the!la specimen.

2.3. Failure assessment

Acoustic emission (AE) was used to trace the damage and failure processes. The essence of the method is that the specimen exposed to mechanical load emits acoustic waves from those areas, where failure occurs (e.g., via matrix deformation, fiber pullout etc.). Detecting the emerging sound waves (along with their characteristics) by a proper transducer the failure mode can be estimated. This happens by assigning parameters of the sound wave to well-detectable failure events (for the latter usually microscopic techniques are adopted). Performing the measurements by an array of four AE transducers (location mode) and by measuring the time lag between the arrival of the AE to all transducers the geometrical position of the sound source can be determined in the knowledge of the sound velocity in the material (e.g., [19–21]).

A four-channel Sensophone AED-40/12 instrument (Hungary) was used for the AE measurements. A piezoelectric transducer of A-11 type was attached to the tensile, bending and static fracture specimens. Based on the force-deformation curve and on the physical parameters of the sound waves (amplitude, rise time, number of oscillations within the events, signal width) various failure modes were assigned to the different amplitude levels.

For the location studies SEN-T specimens of increased width (length × width × thickness = 150 × 70 × 3 mm^3) were used. Width increment was necessary to attach the transducers onto the surface of the specimens and thus to collect and locate the AE signals *in-situ*, i.e. during loading of the SEN-T specimens. As a result of the AE location both planar (2D) and three-dimensional (3D) location maps were constructed, by which the size of the damage zone could be determined by the method proposed by us earlier [22, 23].

The fracture surfaces of the specimens were inspected in a scanning electron microscope (SEM; Jeol JSM-5400, Japan). The studied surfaces were coated with a Au/Pd alloy prior to SEM to avoid static charging.

2.4. Interphase

To detect the morphology of the matrix and the interphase in the composites an atomic force microscope (AFM, Nanoscope of Digital Instruments; USA) equipped with nanoindentation possibility was used. After polishing and ion-etching of the surfaces [8] AFM scans were taken in tapping mode. Making use of a Hysitron Triboscope unit of the AFM instrument, the nano-indentation hardness of the composite constituents was also studied. This allowed us also to estimate the extension of the interphase region. During nano-indentation a needle with a pyramidal ceramic head is pressed into the material whereby its hardness and elastic modulus (E_H) can be determined from the recorded force – indentation depth diagram [24] through Equation 2:

$$E_H = \frac{\sqrt{\pi}}{2\sqrt{A_{hc}}} S_h \tag{12}$$

where A_{hc} is the indentation area determined from the indentation depth and the geometry of the indentor, S_h is the slope of the load recovery hysteresis curve.

3. Results and discussion

3.1. Static mechanical tests

The results of the tensile, three point bending and static fracture mechanical tests, performed at room temperature and 1 mm/min deformation rate, are summarized in Table II. Note that the BFs do not increase the strength of the composites compared to the matrix without surface treatment. So, the reinforcing efficiency of BFs strongly depends on their surface treatment. The strength and modulus values of the composites were both significantly improved by VS and ES treatments. This suggests that the surface treatment changed the initial IPN morphology in the neighborhood of BF. Here the fibers may be embedded into VE- or EP-rich phases if VS and ES treatments, respectively, were applied.

One can also see by collating the results in Table II that in the case of VE, VE/EP 1/1 and VE/EP 3/1 matrices VS treatment is more effective than ES treatment. For the VE/EP=1/3 ratio, however, ES treatment yielded better mechanical properties. So, for a VE-rich hybrid resin VS-treatment, while for EP-rich systems ES-sizing of the fibers seem to be straightforward, at least in the first approximation. This finding should be related with the actual IPN morphology of the hybrid resins [15]. The efficiency of the BF surface treatment can be well observed on SEM micrographs taken from the fracture surfaces. Fig. 1. compares the fracture surfaces of specimens containing non-treated (a) and with VS-treated BFs (b). One can be observe that in absence of surface treatment the resin does not fully cover the BFs and typical failure events are fiber-pullout and debonding. In the case of VS treatment a strong interfacial adhesion appears between the BF and the resin (cf. Fig. 1b). For the composites with hybrid resin matrices the best results were obtained at a VE/EP ratio of 1/1, followed by ratios of 3/1 and 1/3. As speculated above, this behaviour is likely linked with the IPN morphology and its change due to the sized fibers.

3.2. Dynamic mechanical tests

The results of Charpy and falling weight impact tests are summarized in Table III. The related data show similar tendencies as those obtained under static loading conditions. The low fracture energy (a_{cN}) of the VE matrix is obvious. It was markedly enhanced by hybridization with EP. Fig. 2 shows the fracture surfaces of VE (a) and VE/EP (b) systems. The great difference between the fracture modes can be assigned to the IPN structure present in VE/EP. While VE undergone brittle fracture, the VE/EP at the composition ratio of 1/1 failed in a very ductile manner (see "shear steps" on the corresponding fracture surface). The latter is due to the fact that IPN structuring favors the shear deformation which is the major energy dissipation mechanism in thermosets.

TABLE II Static mechanical properties of VE and VE/EP matrix-based composites reinforced with surface treated basalt fibers

	$\sigma_{tensile}$(MPa)	$E_{tensile}$(GPa)	$\sigma_{bending}$(MPa)	$E_{bending}$(GPa)	K_{ICstat}MPam$^{1/2}$)
K1	48.5 ± 3.2	3.3 ± 0.2	70.1 ± 3.9	3.3 ± 0.3	2.3 ± 0.2
K2	46.7 ± 4.0	4.0 ± 0.4	78.6 ± 7.2	4.7 ± 0.5	2.8 ± 0.2
K3	62.8 ± 5.9	5.1 ± 0.3	100.3 ± 4.4	6.5 ± 0.1	4.0 ± 0.3
K4	51.7 ± 5.3	4.7 ± 0.2	82.8 ± 7.7	5.3 ± 0.5	3.7 ± 0.2
K5	41.2 ± 4.4	2.3 ± 0.1	76.7 ± 2.2	2.5 ± 0.1	2.5 ± 0.1
K6	54.2 ± 1.4	3.8 ± 0.1	90.4 ± 9.8	3.5 ± 0.3	3.0 ± 0.1
K7	71.0 ± 6.1	4.3 ± 0.3	125.8 ± 7.1	4.5 ± 0.4	4.2 ± 0.3
K8	70.1 ± 6.5	4.4 ± 0.1	129.6 ± 9.2	4.7 ± 0.2	3.9 ± 0.3
K9	45.3 ± 3.8	2.9 ± 0.1	75.2 ± 3.4	3.0 ± 0.2	2.5 ± 0.2
K10	48.1 ± 3.8	3.5 ± 0.2	83.6 ± 3.3	4.0 ± 0.3	2.6 ± 0.3
K11	64.3 ± 4.3	4.7 ± 0.4	113.1 ± 6.8	6.1 ± 0.3	3.6 ± 0.2
K12	53.6 ± 2.7	4.3 ± 0.2	95.9 ± 8.0	5.1 ± 0.4	3.4 ± 0.2
K13	32.7 ± 2.3	1.4 ± 0.1	56.1 ± 2.3	2.0 ± 0.1	2.2 ± 0.1
K14	41.4 ± 1.4	3.0 ± 0.1	84.5 ± 5.5	3.3 ± 0.2	2.6 ± 0.2
K15	51.7 ± 0.9	3.3 ± 0.1	100.2 ± 5.9	4.0 ± 0.3	3.8 ± 0.1
K16	61.4 ± 2.5	3.9 ± 0.1	113.7 ± 3.4	4.3 ± 0.2	4.0 ± 0.2

TABLE III Dynamic mechanical properties of VE and VE/EP matrix-based composites reinforced with surface treated basalt fibers

	K_{ICdyn} (MPam$^{1/2}$)	G_{IC}(kJ/m^2)	a_{cN}(kJ/m^2)	D_r(%)	E_p(J/mm)
K1	2.7 ± 0.0	2.7 ± 0.3	1.9 ± 0.0	39.9 ± 0.8	0.8 ± 0.0
K2	3.9 ± 0.4	2.9 ± 0.3	3.6 ± 0.2	43.6 ± 3.3	2.0 ± 0.2
K3	4.1 ± 0.1	3.3 ± 0.4	3.5 ± 0.3	55.6 ± 3.5	2.8 ± 0.1
K4	3.9 ± 0.5	2.8 ± 0.0	3.6 ± 0.3	47.3 ± 4.0	2.3 ± 0.2
K5	2.2 ± 0.3	2.7 ± 0.3	2.3 ± 0.3	33.9 ± 0.7	0.9 ± 0.1
K6	3.7 ± 0.4	2.8 ± 0.2	4.2 ± 0.5	48.9 ± 4.1	2.3 ± 0.2
K7	4.6 ± 0.5	9.2 ± 0.7	6.8 ± 0.7	66.0 ± 3.9	4.1 ± 0.3
K8	4.2 ± 0.1	8.2 ± 0.8	6.0 ± 0.4	64.2 ± 5.2	3.6 ± 0.3
K9	2.6 ± 0.3	3.3 ± 0.2	2.1 ± 0.1	40.0 ± 1.0	0.9 ± 0.1
K10	3.0 ± 0.3	3.0 ± 0.1	3.0 ± 0.3	44.0 ± 4.0	2.2 ± 0.2
K11	4.0 ± 0.3	4.1 ± 0.5	3.8 ± 0.4	57.8 ± 2.7	3.5 ± 0.2
K12	3.6 ± 0.3	2.9 ± 0.1	3.0 ± 0.3	51.7 ± 3.4	2.7 ± 0.2
K13	1.9 ± 0.1	2.8 ± 0.0	1.9 ± 0.0	31.0 ± 0.5	0.8 ± 0.1
K14	2.9 ± 0.1	3.1 ± 0.4	3.1 ± 0.4	34.5 ± 2.6	1.5 ± 0.2
K15	4.0 ± 0.4	3.5 ± 0.1	4.2 ± 0.3	47.9 ± 2.8	2.3 ± 0.2
K16	4.4 ± 0.3	6.1 ± 0.3	4.4 ± 0.2	52.1 ± 2.3	3.1 ± 0.3

Outstanding dynamic properties exhibited the composites K7 and K8 likely owing to the "ideal" IPN structure at VE/EP=1/1 ratio and to the VS and ES treatment of BF, respectively. This conclusion is suggested also by the macrophotographs taken from the fractured specimens after falling weight impact tests (Fig. 3). Note that most of the composites failed either at the clamping (Fig. 3a and b), or along the surface of the falling dart (Fig. 3d.), the VE/EP=1/1 matrix-based composites with treated BF failed by radial splitting (in a rose-like manner — see Fig. 3c.). This failure mode is typical for high impact strength, high energy absorbing composites. It can also be observed in Fig. 3d that the excess of the EP component in the hybrid resin formulation results in a more ductile behavior (especially in the presence of ES treatment). This is well reflected by

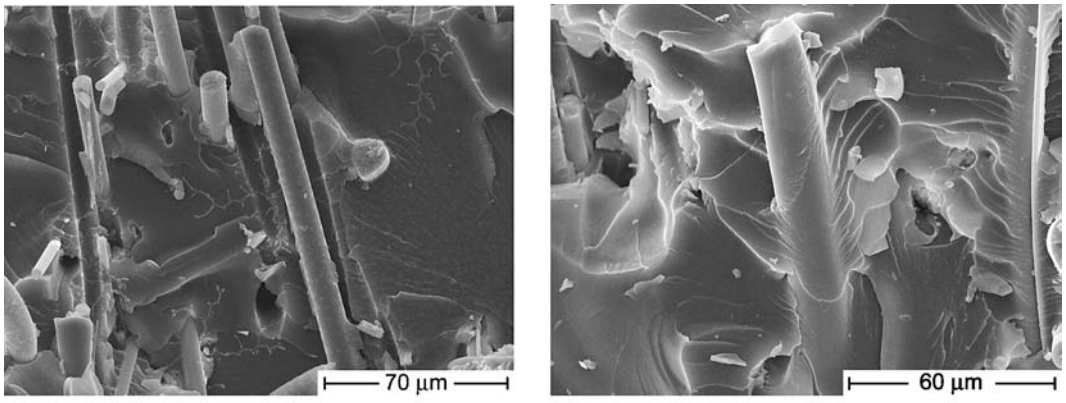

Figure 1 SEM micrographs of the fracture surfaces of the composites with VE/EP (1/1) matrix reinforced with non-treated (a) and VS-treated (b) basalt fibers.

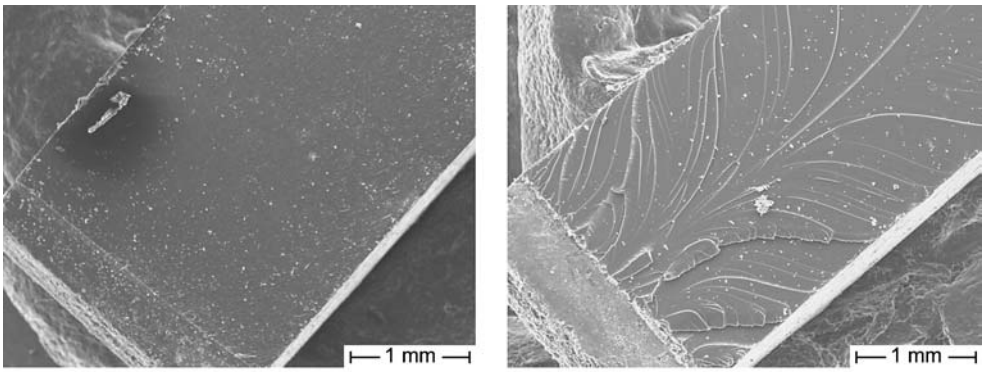

Figure 2 Fracture surfaces of VE(a) and VE/EP = 1/1(b) systems.

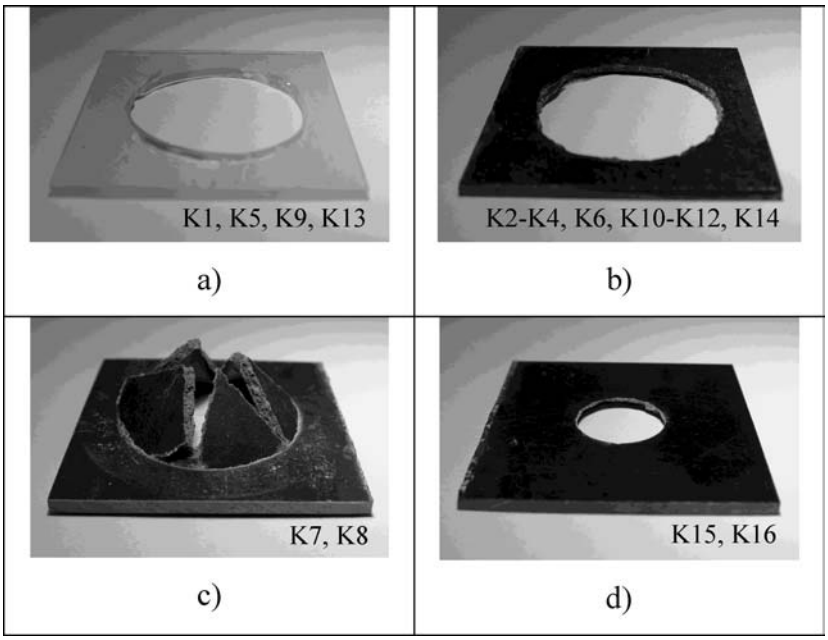

Figure 3 Typical microphotographs taken from BF mat-reinforced VE and VE/EP matrix-based composites after falling weight impact tests. (*Note:* in the right corner of the photographs the codes of those composites are listed which failed according to shown failure mechanisms.)

the improved dynamic properties and in a change of the failure mode (circumferential breakage along the dart).

3.3. Damage and failure based on AE results

The number of AE events detected during the tensile and bending tests is the lowest for the pure matrices and the highest for surface treated BF-reinforced composites. Variations in the surface-treating agents and in the resin hybridization ratio did not cause any significant difference in the number and characteristics of the acoustic signals. The SEN-T specimens of the pure matrices produced low, if any, acoustic activity. The typical amplitude range belonging to matrix fracture was between 40 and 50 dB. The force-displacement curves were divided into four sections by considering the load maximum. Based on our earlier studies (e.g., [25–27]) it is straightforward to select the following stages: 0–0.5F_{max}; 0.5F_{max}–0.8F_{max}; 0.8F_{max}-F_{max} and F_{max}-0. Note that the latter section represents the post-maximum range where crack propagation takes place. The number and amplitude distribution of the acoustic events were investigated in the corresponding pre- and postmaximum ranges. The composites K2, K3, K4, K6 and K10 in the range four (i.e. F_{max}-0) did not produce any AE signals, they failed in a brittle manner after reaching the maximum force. This behavior is the prerequisite of the applicability of the linear elastic fracture mechanics, i.e. determination of the fracture toughness. For the composites K11, K12, K14, and K16 a minimal acoustic activity was found in range four, but the number of the related events was much smaller than in range three (i.e. 0.8 F_{max}-F_{max}). So, these composites failed also brittlely. Composites K7 and K8 had a high number of acoustic events in range four. This indicates pronounced crack propagation and thus ductile failure behavior. In Figs 4 and 5 the amplitude distributions of VE and VE/EP (1/1) matrix-based composites reinforced with VS- and ES-treated BFs are depicted. Based on Figs 4 and 5 one can conclude that resin hybridization decreased the amplitudes by about 10 dB as compared to the pure VE matrix. This is owing to the good damping properties of the IPN-structured VE/EP system. It is worth mentioning that all thermoset IPNs

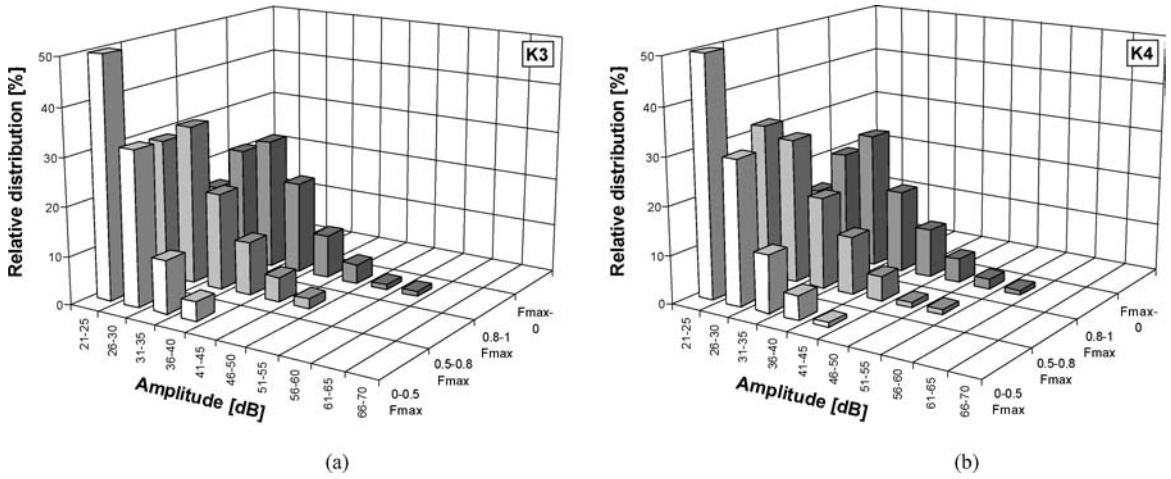

Figure 4 AE amplitude distribution of VE matrix composites reinforced with VS- (K3) (a) and ES-treated (K4) (b) basalt fibers as a function of the loading stages.

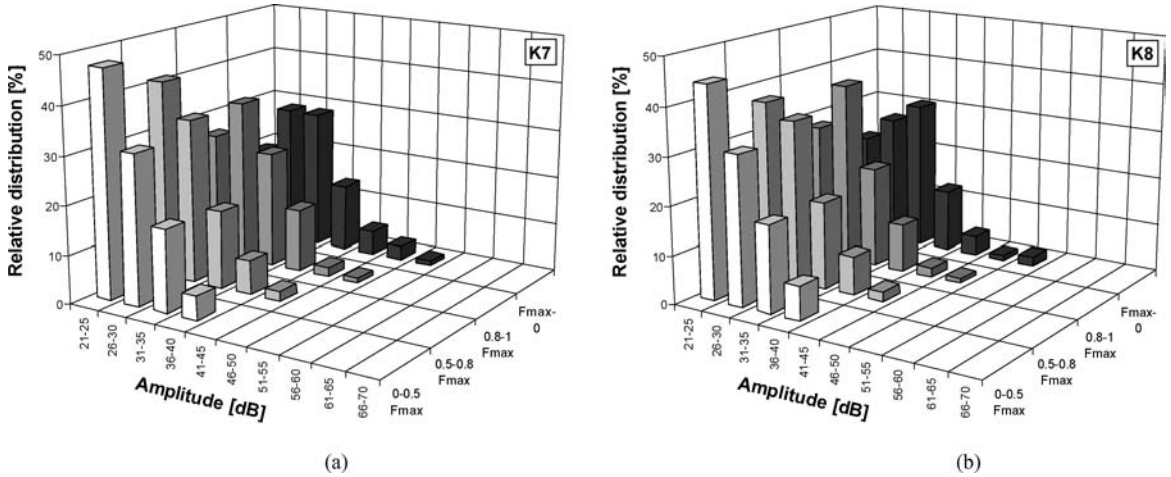

Figure 5 AE amplitude distribution of VE/EP 1/1 matrix composites reinforced with VS- (K7) (a) and ES-treated (K8) (b) basalt fibers as a function of the loading stages.

exhibit an intense and very broad primary relaxation peak (glass transition range) associated with high mechanical and thus acoustic damping, e.g., [9].

In order to determine the size of the damage zone, the AE events were located by a four transducers' array. The related SEN-T specimens undergone brittle fracture with the exception of the composites K7 and K8. The only difference between the two composites containing VE/EP (1/1) matrix was in the surface treatment of the basalt fibers. However, no detectable difference in the shape and size (444 and 469 mm^2) of the damage zone of these composites was found (see Fig. 6).

In respect with the sound velocities the propagation rate was markedly higher in the VE matrix-based composites (2900–3100 m/s) than in the VE/EP (1/1) based ones (2000–2200 m/s). This fact is in line with the above claim, viz., the IPN structured matrix possesses higher acoustic damping properties.

Simultaneously with the AE location the crack propagation was monitored with a digital video camera. The related frame sequences confirmed the findings received by the AE location method. In samples K1-K6, K9, K10 no crack propagation was detected. Specimens of K11, K12, K14-K16 have shown limited crack

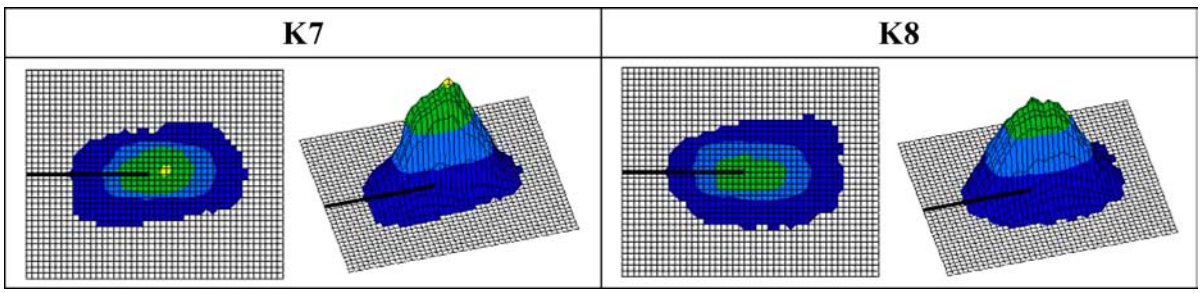

Figure 6 AE location maps of VE/EP (1/1) matrix-based basalt fiber reinforced composites. (*Note*: the notch in the SEN-T specimens is indicated (the size of one unit square is 1 mm^2).)

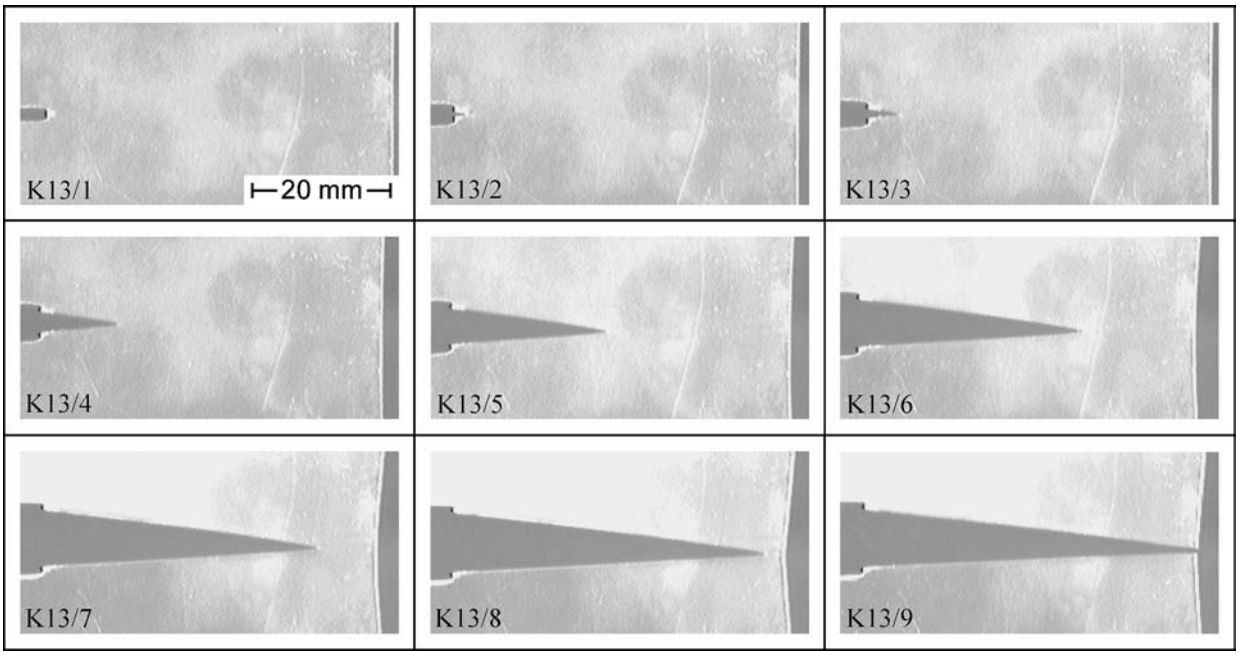

Figure 7 Crack propagation sequence for a VE/EP (1/3) system (K13).

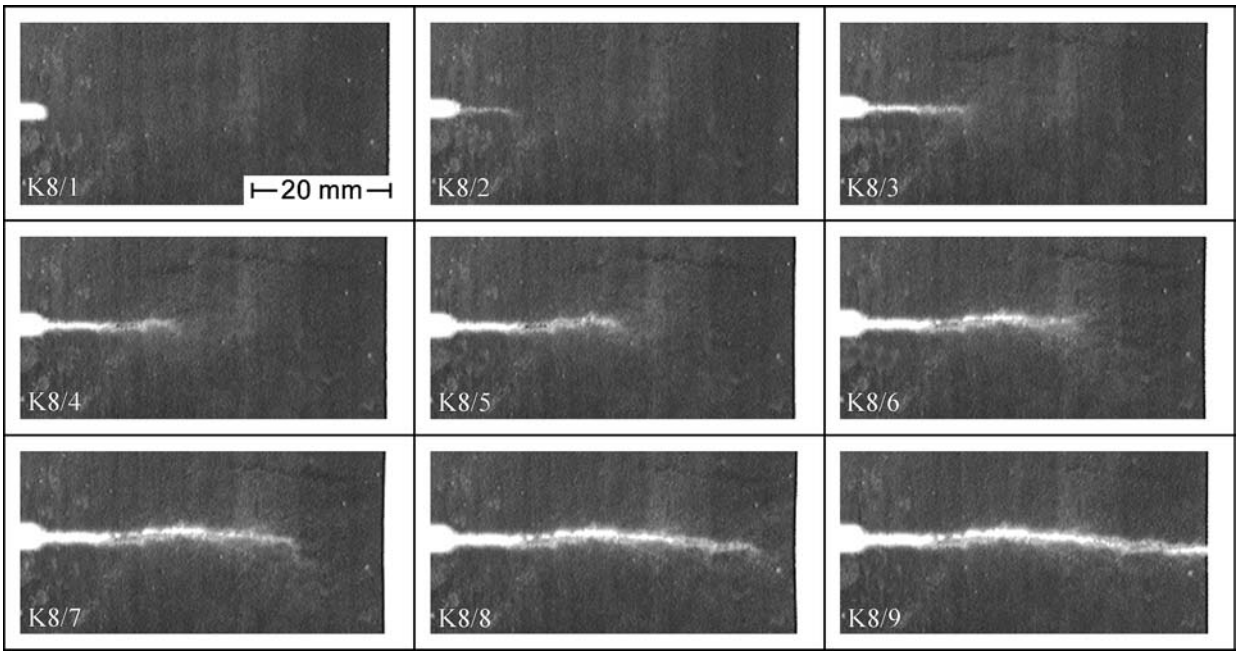

Figure 8 Crack propagation in a VE/EP (1/1) matrix-based ES-treated BF mat-reinforced composite (K8).

propagation (6–10 mm) prior to final brittle fracture. Crack propagation along the full ligament length of the SEN-T specimens was observed only for K7, K8 and K13 (see Figs 7 and 8). These figures demonstrate well the fracture process: after an initial crack opening the crack is blunted, then the crack propagates at a uniform rate through the full ligament of the specimen. Plotting the force-deformation curves for K13 and K8 (see Fig. 9) the ductile behavior of these composites becomes obvious. This ductile failure along with stable crack propagation are due to the interplay between the IPN structure and surface treatment of the BF. This note holds especially for the VE/EP (1/1) matrix-based composites containing VS- or ES-coated BF mats.

3.4. Interphase

In order to elucidate whether the surface treatment of the BF changed the IPN structure of the VE/EP hybrid resin, atomic force microscopy (AFM) equipped with a nanoindenter unit was used. The specimens were ion-etched after polishing. During ion-etching the fact was exploited that the "softer" EP phase is much less resistant to Ar+ bombardment than the "hard" VE [8].

SEM micrographs taken from fracture surfaces already indicated that the BF surface treatment influenced the fiber/matrix adhesion (cf. Fig. 1). This was in agreement with the observed improvement in the mechanical properties. The interphase formed between the fiber and the matrix transfers the load from the "weak"

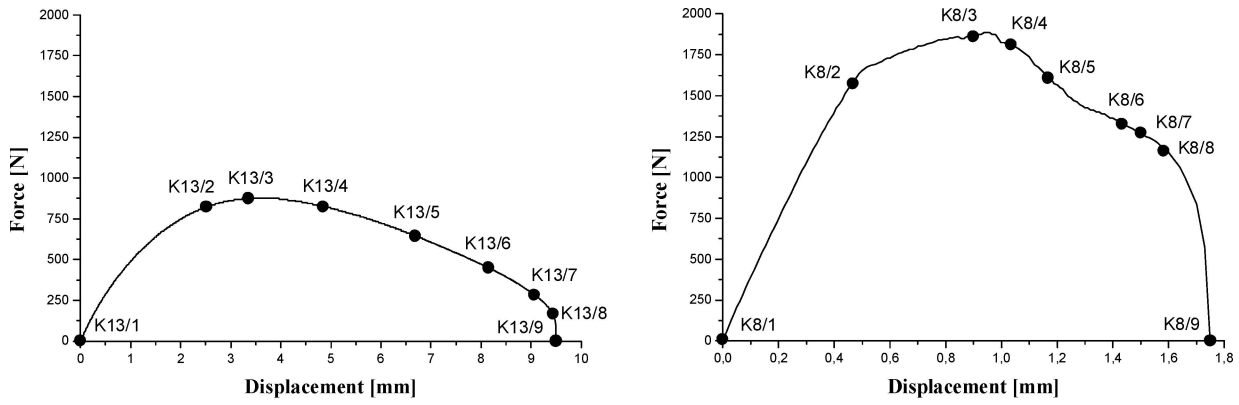

(a) (b)

Figure 9 Force-displacement diagrams of SEN-T specimens cut of a hybrid resin (a –K13) and an ES-treated BF mat-reinforced hybrid resin composite (b –K8). (*Note*: numbers indicated correspond to the sequential crack growth shown in Figs 7 and 8, respectively.)

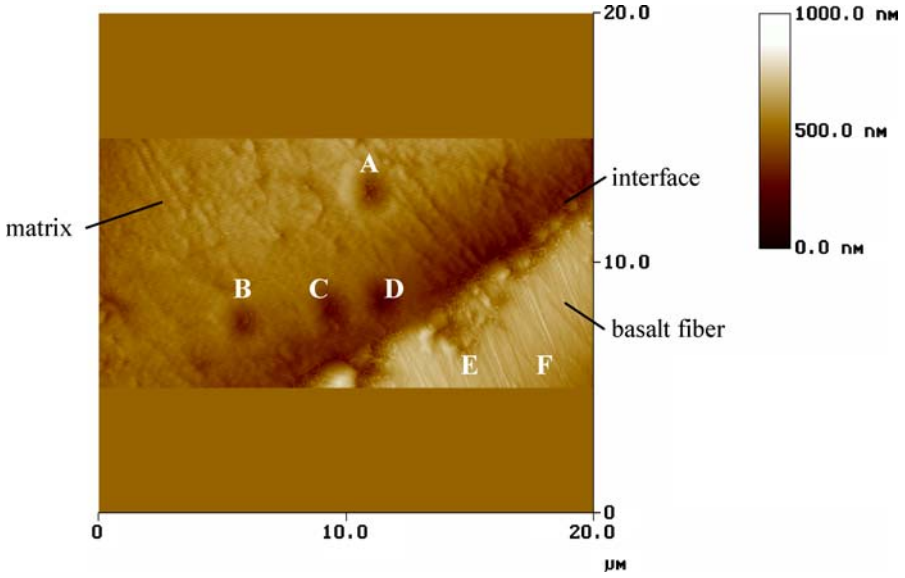

Figure 10 Surface of VE/EP matrix-based ES-treated BF mat-reinforced composite (K8) prepared for nano-indentation test by ion etching. (*Note*: nanoindentation hardness tests were performed at the imprints indicated by letters (A: bulk, B–D: interphase, E–F: BF))

matrix to the "strong" fiber. Nano-indentation studies were conducted on composites containing VE/EP (1/1) matrix and ES-treated BF mat reinforcement. The reason for this choice is that the elastic modulus of EP is lower than that of VE in this case. So, if the interphase contains excess EP with respect to the bulk IPN, then the moduli determined by nano-indentation tests should first decrease (in the interphase) and then increase when moving from the bulk to the BF. This allows us a more precise mapping of the interphase instead of using VS-treated BF where a monotonous increase in the hardness (or modulus) is expected.

Fig. 10 shows the ion-etched surface of the composite sample K8 prepared for the nano-indentation test. The figure clearly shows that, due to the Ar^+ ion etching the immediate environment of the BF is eroded away (a deep valley appears). Recall that EP component used is much less resistant to the Ar^+ ion etching than the VE. This finding corroborates our previous speculation, viz. the EP phase is enriched in the neighborhood of ES-sized BF. It can also be seen in Fig. 10 that the approximate thickness of the interphase is about 2–2.5 μm. The elastic moduli of the composite K8 was determined at points indicated by letters A–F in the figure at a slow, constant indentation rate. From these measurements 2.9 GPa was obtained for the matrix, 1.8 GPa for the interphase and 62 GPa for the BF which are in good correlation with the results of our mechanical tests.

4. Summary

The (fracture) mechanical and failure behavior of discontinuous basalt fiber (BF) reinforced, vinylester (VE) and vinylester/epoxy (VE/EP) matrix-based composites have been studied as a function of resin hybridization and BF surface treatment. It was demonstrated that the toughness of the brittle VE was effectively improved by hybridizing with a suitable EP resin. The VE/EP hybrids in the studied range possess an interpenetrating network (IPN) structure, as shown in Ref. [15], which may be very advantageous in fiber-reinforced composites.

It has been shown that the mechanical properties of the corresponding composites could be strongly

improved by treating the BF with vinyl- or epoxy-containing silanes (VS or ES, respectively). This was traced to a common effect of the IPN structure of the matrix, and good bonding between BF and matrix via the formation of a suitable interphase. Further, the resin transfer molding (RTM) technology, adopted to produce the composite plates, was helpful to avoid the breakage of the BFs.

It was established that for the ratio of 1/1 VE/EP hybrid resin-based composites both strength and toughness could be enhanced at the same time when using surface treated BFs at the right composition of VE/EP. The shape and size of the damage zone in the composites detected by location of the acoustic emission (AE) activity proved to be independent of the type of BF surface treatment and of the resin composition.

Acknowledgements

This work was supported by Hungarian Ministry of Education (NKFP 3A/0036/2002) and Hungarian-German Intergovernmental Science and Technology Program (TéT D-16/02; HUN 02/024). Part of this work was supported by the German Science Foundation (DFG). J. Karger-Kocsis thanks the Fonds der Chemischen Industrie for the support of his personal research.

References

1. A. R. BUNSELL, in "Fibre Reinforcements for Composite Materials" (Elsevier, New York, 1988).
2. D. GAY, S. V. HOA and S. W. TSAI, in "Composite Materials, Design and Applications" (CRC Press, New York, 2003).
3. W. B. GOLDSWORTHY, *Compos. Technol.* **8** (2000) 15.
4. T. CZIGÁNY, *Mater. Sci. Forum.* **473/474** (2005) 59.
5. T. G. GUTOWSKY, in "Advanced Composites Manufacturing" (Wiley & Sons, New York, 1997).
6. P. I. BASHTANNIK, A. I. KABAK and Y. Y. YAKOVCHUK, *Mech. Compos. Mater.* **39** (2003) 85.
7. G. LUBIN, in "Handbook of Composites" (Van Nostrand Reinhold Publisher, New York, 1982).
8. J. KARGER-KOCSIS, O. GRYSHCHUK and S. SCHMITT, *J. Mater. Sci.* **38** (2003) 413.
9. *Idem.*, in Phase Morphology and Interfaces in Micro- and Nanostructured Multiphase Polymer Systems edited by G. Harrats, G. Groeninckx and S. Thomas (Marcel-Dekker, Francis and Taylor Boca Raton, FL, 2005) in press.
10. O. GRYSHCHUK and J. KARGER-KOCSIS, *J. Polym. Sci. Part A-Chem.* **42** (2004) 5471.
11. A. G. ATKINS, *J. Mater. Sci.* **10** (1975) 819.
12. Y. W. MAI and F. CASTINO, *ibid.* **19** (1984) 1638.
13. J. S. SZABÓ, G. ROMHÁNY, T. CZIGÁNY and J. KARGER-KOCSIS, *Adv. Compos. Lett.* **12** (2003) 113.
14. J. S. SZABÓ, J. KARGER-KOCSIS, O. GRYSHCHUK and T. CZIGÁNY, *Compos. Sci. Technol.* **64** (2004) 1717.
15. O. GRYSHCHUK and J. KARGER-KOCSIS, *J. Nanosci. Nanotechnol.* (submitted)
16. K. FRIEDRICH, in "Application of Fracture Mechanics to Composite Materials" (Elsevier Science Publisher, Amsterdam, 1989).
17. J. G. WILLIAMS, in "Fracture Mechanics of Polymers" (Ellis Horwood, New York, 1987).
18. T. M. LIU and W. E. BAKER, *Polym. Eng. Sci.* **31** (1991) 753.
19. M. ASTY, *NDT Intern.* **11** (1978) 223.
20. V. KIVIBODROV, *J. Aco. Em.* **13** (1995) 87.
21. M. WEVERS and M. SURGEON, in Comprehensive Composite Materials, edited by A. Kelly and C. Zweben (Elsevier, New York, 2000).
22. T. CZIGÁNY and J. KARGER-KOCSIS, *Polym. Polym. Compos.* **1** (1993) 329.
23. J. KARGER-KOCSIS, T. CZIGÁNY and J. MAYER, *Plast. Rubb. Compos.* **25** (1996) 109.
24. W. C. OLIVER and G. M. PHARR, *J. Mater. Res.* **7** (1992) 1564.
25. J. KARGER-KOCSIS and T. CZIGÁNY, *J. Mater. Sci.* **28** (1993) 2438.
26. T. CZIGÁNY and J. KARGER-KOCSIS, *Polym. Bull.* **31** (1993) 495.
27. T. CZIGÁNY, Z. A. MOHD ISHAK, T. HEITZ and J. KARGER-KOCSIS, *Polym. Compos.* **17** (1996) 900.

Received 3 December 2004
and accepted 30 March 2005